CELL BIOLOGY

# Mad3 modulates the $G_1$ Cdk and acts as a timer in the Start network

**Alexis P. Pérez[1,2], Marta H. Artés[1], David F. Moreno[1], Josep Clotet[2]*, Martí Aldea[1,2]***



**Cells maintain their size within limits over successive generations to maximize fitness and survival. Sizer, timer, and adder behaviors have been proposed as possible alternatives to coordinate growth and cell cycle progression. Regarding budding yeast cells, a sizer mechanism is thought to rule cell cycle entry at Start. However, while many proteins controlling the size of these cells have been identified, the mechanistic framework in which they participate to achieve cell size homeostasis is not understood. We show here that intertwined APC and SCF degradation machineries with specific adaptor proteins drive cyclic accumulation of the $G_1$ Cdk in the nucleus, reaching maximal levels at Start. The mechanism incorporates Mad3, a centromeric-signaling protein that subordinates $G_1$ progression to the previous mitosis as a memory factor. This alternating-degradation device displays the properties of a timer and, together with the sizer device, would constitute a key determinant of cell cycle entry.**

## INTRODUCTION

The scale and efficiency of most molecular processes that take place within a cell depend on its size. Hence, as an important factor of fitness and survival, cell size is maintained within constant limits under unperturbed conditions of growth (*1*–*4*). In budding yeast, although cells show a size checkpoint at the $G_2$-M transition (*5*–*7*), they primarily control their size before S-phase entry at a point termed Start (*8*, *9*), where cell size displays the lowest variability compared to other cell cycle transitions.

In principle, size homeostasis can be attained by means of three different model mechanisms: sizers, timers, and adders (*10*). A sizer allows cells to test their size and can be based on accumulation of inducers or dilution of inhibitors of cell cycle entry as cells grow. Timers are able to trigger a molecular event as a function of time, and they may be originated by enzymatic reactions functioning at saturation. Last, the adder allows cells to measure a fixed size increment and may emanate from the combination of molecular mechanisms acting as timers and sizers (*11*, *12*). However, available experimental evidence addressing whether $G_1$ is controlled by sizer, timer, or adder mechanisms is inconclusive in yeast (*13*–*15*) and mammalian cells (*16*).

Cyclin Cln3 is the most upstream activator of Start (*17*). This $G_1$ cyclin forms a complex with Cdc28, the cell cycle cyclin-dependent kinase (Cdk) in budding yeast, to activate transcription of the $G_1$-S regulon (*18*) by phosphorylation of RNAPolII C terminus (*19*), where *CLN1* and *CLN2*, two additional $G_1$ cyclins under the control of Whi5, create a positive feedback loop that makes Start a robust and irreversible transition (*20*). Alteration of key molecules of the Start network has prominent effects on the critical size (*21*). In particular, Cln3 and Whi5 modulate cell size in a precise dose-dependent manner. Whi5 is synthesized during the previous cycle independently of cell mass and is diluted by growth in $G_1$ (*22*), thus offering the key properties to function as a sizer molecule at Start (*11*, *23*). The Cln3 cyclin is present at low but nearly constant levels throughout $G_1$ (*17*, *24*), and its nuclear accumulation depends on Hsp70/Hsp40 chaperone systems and the Cdc48 segregase (*25*–*27*), which would be important for subjugating cell cycle entry to growth rate and aging (*14*, *28*, *29*). Cln3 is recruited to $G_1$-S promoters, and its titration as a function of the mass/DNA ratio has been proposed as a sizer mechanism (*30*). Nonetheless, no evidence exists showing that changes in Cln3 levels or subcellular distribution during $G_1$ play a role in a sizer or timer mechanism.

Here, we analyze the mechanisms regulating nuclear accumulation of Cln3 during $G_1$ progression and entry into the cell cycle, and we find that Mad3, a nuclear centromeric-signaling factor (*31*), plays an active role in by Skp1–Cullin–F-box (SCF) degradation of Cln3 in the nucleus. In turn, Mad3 levels decrease during $G_1$ by anaphase-promoting complex (APC)–dependent degradation, thus raising the nucleocytoplasmic ratio of Cln3 as cells progress in $G_1$ to reach a maximal level at cell cycle entry. Our results reveal a new regulatory layer in $G_1$ control and provide a mechanism with a timer behavior in the Start network.

## RESULTS

### Cyclin Cln3 accumulates in the nucleus in $G_1$ and peaks during entry into the cell cycle

We previously observed by indirect immunofluorescence methods a prominent nuclear signal of Cln3 when cells enter the cell cycle (*26*, *32*). To characterize the temporal dynamics of this phenomenon, we decided to monitor $G_1$ cyclin localization in live cells during $G_1$ progression by time-lapse microscopy. Cln3 is too short-lived to be detected as a fluorescent-protein fusion in single cells unless partially stabilizing mutations are used (*22*, *33*). To avoid premature entry into the cell cycle caused by elevated $G_1$ cyclin levels, a hypoactive mutation in the cyclin box was also introduced that maintains size within a physiological range. As previously described (*22*), mCit-$Cln3^{11A}$ displayed a distinct nuclear signal in most asynchronously growing cells. However, after careful measurement of images obtained by wide-field fluorescence microscopy (fig. S1A), we observed that nucleocytoplasmic ratios of mCit-$Cln3^{11A}$ increased during $G_1$ progression and reached maximum values at budding (Fig. 1, A to C), thus confirming previous observations obtained with 3HA-tagged wild-type Cln3 by immunofluorescence (*32*). To support the nucleocytoplasmic ratio data, we also directly measured the nuclear

[1]Molecular Biology Institute of Barcelona (IBMB), CSIC, 08028 Barcelona, Catalonia, Spain. [2]Department of Basic Sciences, Universitat Internacional de Catalunya, 08195 Sant Cugat del Vallès, Spain.
*Corresponding author. Email: jclotet@uic.es (J.C.); marti.aldea@ibmb.csic.es (M.A.)

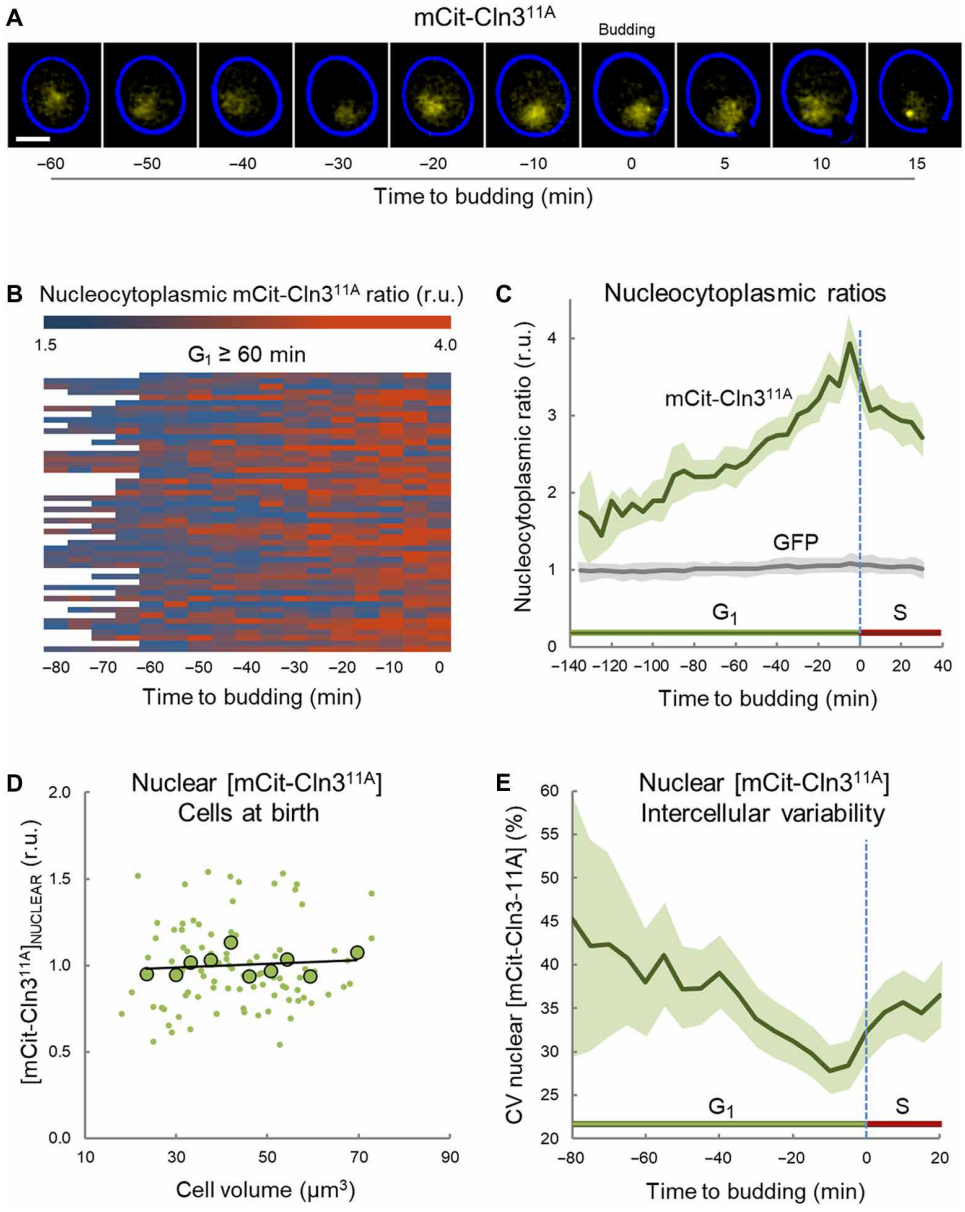


**Fig. 1. Cln3$^{11A}$ accumulates specifically in the nucleus during $G_1$ and reaches a maximum around Start.** (**A**) Cells expressing mCit-Cln3$^{11A}$ were analyzed by wide-field time-lapse microscopy during $G_1$ progression and entry into the cell cycle. The fluorescence signal of mCit-Cln3$^{11A}$ (yellow) and the bright-field contour (blue) from a representative cell at different times relative to budding are shown. Scale bar, 2 μm. (**B**) Heatmap displaying nucleocytoplasmic ratios of mCit-Cln3$^{11A}$ during $G_1$ and entry into the cell cycle. Data in relative units (r.u.) were obtained from single cells ($N = 50$) every 5 min and aligned to budding time. (**C**) Nucleocytoplasmic ratio of mCit-Cln3$^{11A}$ in $G_1$ cells as in (A) aligned to budding. Relative mean ± SE values ($N = 100$) are plotted. Data obtained from GFP-expressing cells are shown as control. (**D**) Nuclear concentration of mCit-Cln3$^{11A}$ in cells at birth as a function of cell volume. Relative single-cell ($N = 100$, small circles) and binned data ($N = 10$, large circles) with the corresponding regression line are plotted. (**E**) Intercellular variability of nuclear mCit-Cln3$^{11A}$ concentration during $G_1$ and entry into the cell cycle. Coefficient of variation ± SE values of nuclear mCit-Cln3$^{11A}$ concentration are plotted as a function of time to budding.

concentration of mCit-Cln3$^{11A}$ by confocal time-lapse microscopy and obtained comparable results (fig. S1, C to E) to those by wide-field microscopy (fig. S1B). The nuclear concentration of mCit-Cln3$^{11A}$ did not change significantly with cell size at birth (Fig. 1D), suggesting that Cln3 is passively segregated during cell division, likely because of free diffusion between mother and daughter compartments. Last, intercellular variability of the nuclear concentration of mCit-Cln3$^{11A}$ decreased during $G_1$ and reached a minimum about 10 min before budding (Fig. 1E), which points to nuclear levels of Cln3 as a likely key parameter ruling entry into the cell cycle.

Cln3 contains a bipartite nuclear localization signal (NLS) at its C terminus that is essential for proper entry into the cell cycle (*34*, *35*). Since Cdc28 depends on the cyclin Cln3 NLS to accumulate in the nucleus in $G_1$ cells (*32*), we decided to study a Cdc28-GFP (green fluorescent protein) fusion in a wild-type *CLN3* background to test the results observed with the mCit-Cln3$^{11A}$ protein. While total

Whi5-mCherry concentration showed a steady decrease during $G_1$ as described (*22*), overall Cdc28-GFP concentration was kept constant (fig. S2A). However, Cdc28-GFP displayed a progressive accumulation in the nucleus until late $G_1$, with a maximal value at Start as determined by completion of Whi5-mCherry export, approximately 12 min before budding (Fig. 2, A and B). Notably, the nuclear concentration of Cdc28-GFP correlated ($P < 1 \times 10^{-11}$) with the total concentration of Whi5-mCherry in single cells at Start (Fig. 2C), in which the fitted slope attained maximal values (fig. S2B). As expected, we observed no correlation between the nuclear concentration of Cdc28-GFP and the total concentration of mCherry expressed from a constitutive promoter (fig. S2C). These data support the idea that critical nuclear Cdc28 and Whi5 levels are main determinants of Start, where cells would integrate signals on both the $G_1$ Cdk and the $G_1$-S inhibitor when entering the cell cycle (*22*, *33*). Regarding the role of Cln3, we found that nuclear accumulation of Cdc28-GFP

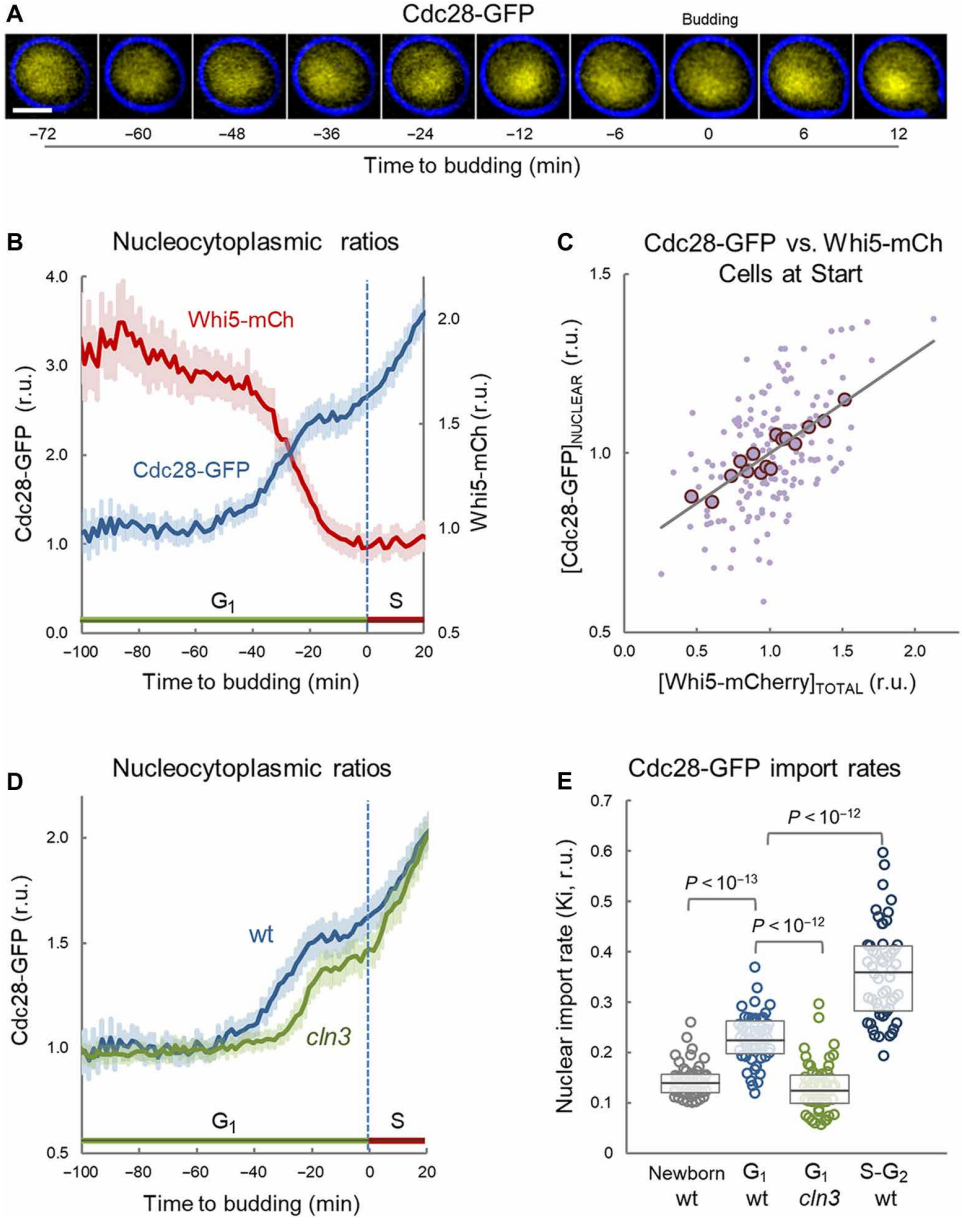


**Fig. 2. Cln3 boosts nuclear import of Cdc28-GFP during cell cycle entry.** (**A**) Cells expressing Cdc28-GFP and Whi5-mCh were analyzed by time-lapse microscopy during $G_1$ progression and entry into the cell cycle. The fluorescence signal of Cdc28-GFP (yellow) and the bright-field contour (blue) from a representative cell at different times relative to budding are shown. Scale bar, 2 μm. (**B**) Nucleocytoplasmic Cdc28-GFP and Whi5-mCh ratios in cells as in (A) aligned to budding. Relative mean ± SE values ($N = 100$) are plotted. (**C**) Nuclear Cdc28-GFP concentration as a function of cellular Whi5-mCherry concentration at Start. Relative single-cell data ($N = 100$, small circles) are plotted. Mean values of binned data ($N = 10$, large circles) and a regression line are also shown. (**D**) Nucleocytoplasmic Cdc28-GFP ratios in wild-type (wt) and Cln3-deficient (*cln3*) cells aligned to budding. Mean ± SE values ($N = 100$) are plotted. (**E**) Nuclear import rates of Cdc28-GFP in individual wild-type (wt) and Cln3-deficient (*cln3*) $G_1$ cells. Data from wt cells in early $G_1$ (newborn) or S-$G_2$-M phases are shown for comparison. Median ($N = 50$) and quartile values are plotted. Pairwise comparisons were performed with a Mann-Whitney *U* test, and the resulting *P* values are indicated.

was delayed in Cln3-deficient cells aligned at budding time, and nucleocytoplasmic ratios of Cdc28-GFP were always lower throughout entry into the cell cycle (Fig. 2D). Likely because of the fact that Cdc28 is present at much higher levels than Cln3 (*17*, *36*), differences in the steady-state nucleocytoplasmic ratio of Cdc28-GFP in late $G_1$ cells were only modest. Thus, we decided to analyze directly the import kinetics of Cdc28-GFP by nuclear fluorescence loss in photobleaching (FLIP) (*28*). We found that the nuclear import rate of Cdc28-GFP required Cln3 and was minimal in early $G_1$ compared to all other stages during $G_1$ progression (Fig. 2E and fig. S2, D and E). Although the Cln3 NLS is essential for its role at Start, Cln1 and Cln2 would likely contribute to Cdc28 import (*37*) once the positive feedback loop is triggered, thus explaining the residual import rate of Cdc28 observed in the *cln3* mutant. Overall, these data are consistent with a posttranslational mechanism that progressively increases the nuclear levels of Cln3 during $G_1$ for the timely execution of Start.

### Cln3 cyclin stability in the nucleus is modulated by Mad3 and increases with cell size in $G_1$ cells

The Cln3 NLS is constitutively active through all stages of the cell cycle (*34*, *35*), and contrary to Cln1 and Cln2 (*37*), Cln3 does not seem to have a nuclear export signal. Thus, we speculated that the posttranslational control of the nuclear levels of Cln3 that we observed could be due to protein stability. Cln3 is ubiquitinated by SCF with the aid of two alternative F-box proteins, Grr1 in the cytoplasm and Cdc4 in the nucleus (*38*), thus pointing to Cdc4 as a putative factor modulating Cln3 stability in the nucleus during $G_1$. The dependence of Cln3 degradation on Cdc4 is almost absolute in the absence of Grr1 (*38*), suggesting that fine-tuning Cdc4 activity by regulatory factors could produce moderate but relevant changes in Cln3 levels in the nucleus. In this respect, we recently identified Mad3 as a nuclear centromeric-signaling protein that increases the critical size when cells contain an exceeding number of centromeres (*39*). During the course of these experiments, we found that Mad3 interacts with Cln3 and Cdc4 and increases nuclear degradation of the $G_1$ cyclin. Thus, we wanted to test whether Mad3 plays a role in the degradation of nuclear Cln3 in $G_1$ phase under normal conditions. As shown in Fig. 3A, while mCit-$Cln3^{11A}$ half-life in wild-type $G_1$ cells was ca. 20 min, degradation kinetics in Mad3-deficient cells were slower, producing a twofold extension in the half-life of mCit-$Cln3^{11A}$. Next, we analyzed degradation rates in $G_1$ at the single-cell level and found a strong negative correlation with cell size in the wild-type strain but not in Mad3-deficient cells in which the degradation rate was constant independently of cell size (Fig. 3B). We found that the nucleocytoplasmic ratio and the concentration of mCit-$Cln3^{11A}$ in the nucleus remained high from early $G_1$ to budding in Mad3-deficient cells (Fig. 3C and fig. S3A). Mad3-deficient cells are smaller at budding (*39*), which is consistent with the idea that, by contributing to degradation of Cln3 during $G_1$, the Mad3 protein acts as an inhibitor of Start. Accordingly, Cln3 was required for the reduction in budding volume caused by a *mad3* deletion (fig. S3B).

Execution of Start not only depends on $G_1$ cyclin levels but also on Whi5 (*22*, *40*, *41*). Unexpectedly, deletion of *MAD3* in Whi5-deficient cells did not cause a further reduction in cell size (fig. S3B). On the other hand, we found no significant changes in Whi5 export kinetics and overall levels at Start when comparing wild-type and Mad3-deficient cells (fig. S3, C and D). Thus, although Mad3 would act specifically to restrain cyclin Cln3, the resulting effects on cell cycle entry would require an intact Start network.

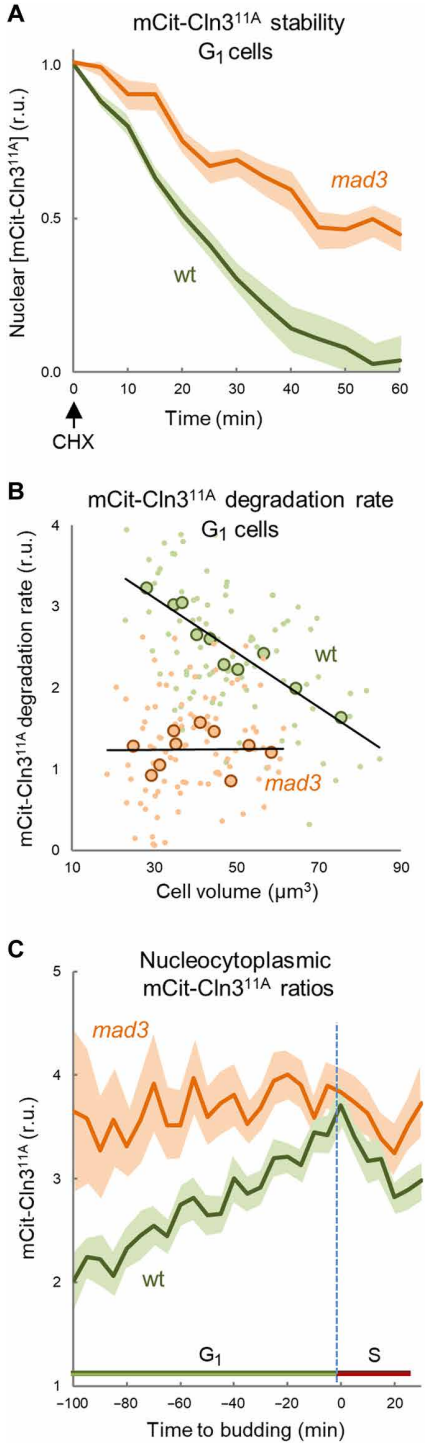


**Fig. 3. $Cln3^{11A}$ stability in the nucleus is modulated by Mad3 and increases with cell size in $G_1$ cells.** (**A**) Analysis of mCit-$Cln3^{11A}$ stability in the nucleus of wild-type (wt) and Mad3-deficient (*mad3*) $G_1$ cells. Nuclear concentrations of mCit-$Cln3^{11A}$ were determined at the indicated times after cycloheximide (CHX) addition. Mean ± SE values ($N = 100$) are plotted. (**B**) Degradation rate of mCit-$Cln3^{11A}$ in wild-type (wt) and Mad3-deficient (*mad3*) $G_1$ cells. Relative single-cell data ($N = 100$, small circles) are plotted. Mean values of binned data ($N = 10$, large circles) and the corresponding regression lines are also shown. (**C**) Nucleocytoplasmic mCit-$Cln3^{11A}$ ratios in wild-type (wt) and Mad3-deficient (*mad3*) cells aligned to budding. Mean ± SE values ($N = 100$) are plotted.

### Mad3 protein levels oscillate during the cell cycle as a function of APC activity

Transcription of *MAD3* and *CDC4* is not cell cycle regulated (*42*), which prompted us to analyze levels of these two proteins when expressed from constitutive promoters during the cell cycle. While a GFP-Cdc4 fusion protein was maintained at constant levels (fig. S4A), mCh-Mad3 levels decreased during $G_1$ progression (Fig. 4, A, B, and D) by posttranscriptional mechanisms (fig. S4B). By contrast, the concentration of mCh-Mad3 progressively recovered during the S-$G_2$-M period in the mother cell compartment and decreased during the last 10 to 15 min because of nuclear division (Fig. 4, C and E). Amounts of the mCh-Mad3 protein were segregated during mitosis following a 1:1 ratio in mother and daughter cells, but because of their smaller size, daughter cells were born with a higher concentration of Mad3 (Fig. 4F), similar to data from early-$G_1$ cells in Fig. 4D. Last, by using fluorescence resonance energy transfer (FRET), we found that levels of the Mad3-Cdc4 complex were proportional to mCh-Mad3 from birth to budding (Fig. 4G and fig. S4C), indicating that Mad3 levels are sufficiently limiting to set the steady-state levels of the Mad3-Cdc4 complex during $G_1$ progression.

Mad3 is an unstable protein that has been shown to be degraded in $G_1$ with the key contribution of the APC and Cdh1 (*43*). Taking into account that $APC^{Cdh1}$ is activated late in mitosis and remains active throughout $G_1$ until entry into S phase, Mad3 stability should be sharply reduced during mitotic exit, thus providing an explanation to the observed progressive decline in Mad3 protein levels during the ensuing $G_1$ phase until the new steady state set by $APC^{Cdh1}$ activation is reached. To test this prediction, we analyzed a Mad3 mutant lacking the KEN30 box that mediates degradation by Cdh1 (*43*) and found that protein concentration at budding was higher compared to wild type (fig. S4D) and, notably, did not decrease during $G_1$ (fig. S4E).

Next, we wanted to test whether Cdh1 is not only necessary but also limiting for Mad3 degradation in $G_1$ cells. As the *CDH1* gene is normally expressed at low levels, we analyzed *GAL1p-CDH1* cells in medium with raffinose to limit *GAL1p* activity to basal levels and attain a low level of expression. These conditions, which caused a moderate 3.2-fold increase in *CDH1* expression over wild-type cells, decreased levels of Mad3 by 2.7-fold in $G_1$ cells and produced a clear reduction in cell size (Fig. 4, H and I), similar to that observed in Mad3-deficient cells (*39*). Confirming the dependence of Mad3 stability on anaphase completion, the concentration of Mad3 readily increased in cells arrested in metaphase by turning off *GAL1p-CDC20* expression (fig. S4F). In summary, these results indicate that Mad3 protein levels oscillate during the cell cycle, reaching a minimum value in daughter cells at the $G_1$-S transition, and point to the cyclic activation $APC^{Cdh1}$ as a new layer of control in the Start network.

We previously observed a spindle-assembly checkpoint (SAC)-dependent delay in mitosis in cells containing an exceeding number of centromeric sequences (*39*), which prompted us to test the effects on Mad3. We found that Mad3 levels increased in newborn cells with centromere-containing plasmids (fig. S4G). Mad3 levels displayed a positive correlation with cell size at birth in cells transformed with three centromeric vectors (fig. S4H), suggesting that longer delays in the previous mitosis up-regulate Mad3 to higher levels. In all, these data point to Mad3 as a sensor of the metaphase-anaphase transition that modulates the duration of the ensuing $G_1$ phase.

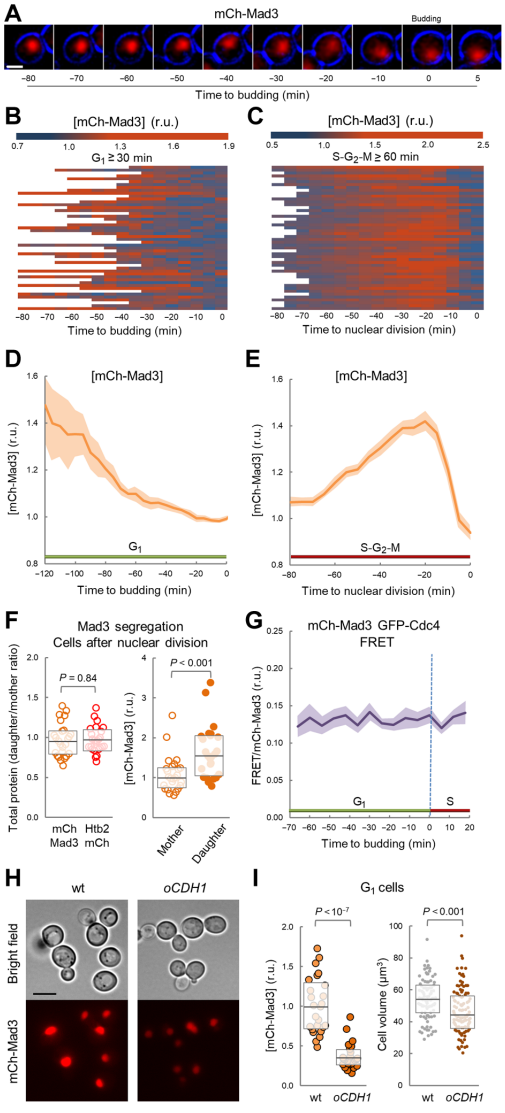


**Fig. 4. Mad3 protein levels oscillate during the cell cycle as a function of APC activity.** (**A**) Cells expressing mCh-Mad3 from a constitutive promoter during $G_1$ progression and entry into the cell cycle. A representative cell at different times relative to budding is shown. Scale bar, 2 μm. (**B** and **C**) Heatmaps displaying mCh-Mad3 concentration during the cell cycle. Relative data from single cells ($N = 50$) were obtained every 5 min and aligned to budding (B) or nuclear division (C). (**D** and **E**) Cellular concentration of mCh-Mad3 in cycling cells as in (A) aligned to budding (D) or nuclear division (E). Relative mean ± SE values ($N = 100$) are plotted. (**F**) Nuclear segregation of mCh-Mad3. Total amounts (left) and concentrations (right) of mCh-mad3 were determined in daughter and mother cell compartments after nuclear division and the corresponding relative data with median ($N = 25$) and quartile values are plotted. Pairwise comparisons were performed with a Mann-Whitney *U* test, and the resulting *P* values are indicated. Histone Htb2 fused to mCherry (Htb2-mCh) was used as control. (**G**) Mad3-Cdc4 interaction efficiency in $G_1$ cells. Cells expressing mCh-Mad3 and GFP-Cdc4 were analyzed by FRET during $G_1$ progression and cell cycle entry. Relative mean ± SE values ($N = 50$) of the inferred Mad3-Cdc4 complex relative to mCh-Mad3 levels in cells aligned to budding are plotted. (**H**) Representative images of cells with empty vector (wt) or expressing a *GAL1p-CDH1* construct (*oCDH1*) in raffinose medium to limit *GAL1p* expression to basal levels. (**I**) Concentration of mCh-Mad3 (left, $N = 25$) and cell volume (right, $N = 100$) in $G_1$ cells as in (H). Single-cell data with the corresponding median and quartile values are plotted. Pairwise comparisons were performed with a Mann-Whitney *U* test, and the resulting *P* values are indicated.

### Mad3 adds a timer component to the mechanisms of $G_1$ cyclin activation at Start

Protein degradation normally follows apparent first-order kinetics determined by a half-life parameter in time units (*44*, *45*) and provides oscillators with robust temporal dynamics (*46*). Thus, we asked whether Mad3 degradation would introduce a time-dependent mechanism in $G_1$ control. Early work in fission yeast established a theoretical framework based on simple cell size measurements to test the existence of timer and sizer mechanisms controlling a cell cycle phase (*47*). Briefly, concerning control of $G_1$ in budding yeast, the increase in size from birth to budding should be independent of the birth size if $G_1$ length is only determined by a timer (Fig. 5A), which would produce a null or positive slope depending on whether linear or exponential growth is considered. By contrast, if the end of $G_1$ is determined by a critical size (Fig. 5B), then cells born with a smaller size than average must increase their size to a larger extent than those born larger, i.e., cell volume extension during $G_1$ would negatively correlate with birth volume and display a slope of −1. However, available experimental data do not univocally discriminate between these two possible scenarios. Wild-type cells of budding yeast display a negative slope, from −0.4 to −0.3 depending on strain background (*13*, *14*) but far from the theoretical −1 value predicted by the sizer mechanism. In agreement with previous data, wild-type cells used in this study displayed a slope of −0.283 in asynchronous cultures (Fig. 5C) and −0.296 in newly born cells (fig. S5A). Notably, Mad3-deficient cells exhibited a slope of −0.835 in asynchronous cultures (Fig. 5D) and −0.773 in newly born cells (fig. S5B), significantly different ($P = 2.10 \times 10^{-4}$) from those obtained from wild-type cells (fig. S5C), which indicates that Mad3 weakens the sizer behavior of $G_1$ control, perhaps by adding a timer mechanism. To analyze this possibility, we used experimental data on cycle time, $G_1$ length and cell volumes at birth and budding, and simulated the dependence of cell volume extension in $G_1$ on birth volume with the aid of a pure sizer model or alternative models wherein the sizer device coexists with either timer or adder mechanisms. To reproduce the observed variability in cell volume and $G_1$ length, experimental coefficients of variation were introduced in the models (Fig. 5, E and F, and data file S1). While sampled simulations of the sizer and adder-sizer models produced median slopes of −1 and −0.49, respectively, the timer-sizer model exhibited a median slope of −0.3, very similar to that obtained from bootstrapped samples of wild-type cells (Fig. 5G). By contrast, the dependence of cell volume extension on birth volume displayed by Mad3-deficient cells was stronger, with a negative slope much closer to that predicted by the pure sizer model. Together, these data point to the notion that Mad3 contributes with a timer behavior to the mechanisms that trigger entry into the cell cycle. Supporting this idea, Mad3 concentration displayed similar average values and variability in cells born with different sizes (fig. S5D), which would rule out a function as a sizer molecule (*23*).

To assess the relative contribution of the sizer and timer mechanisms in cell cycle entry, we analyzed the probability of budding as a function of cell size and time by multivariable logistic regression. We found that both cell volume ($P < 1 \times 10^{-3}$) and time from birth ($P < 1 \times 10^{-3}$) were significant predictors of budding in wild-type cells (Fig. 6, A and C). However, whereas cell volume accurately ($P < 1 \times 10^{-4}$) predicted budding in *mad3* cells, time from birth had no effect ($P = 0.26$) (Fig. 6, B and D).

Last, to test further whether Mad3 degradation could act as a timer, we asked whether degradation and dilution mechanisms would be

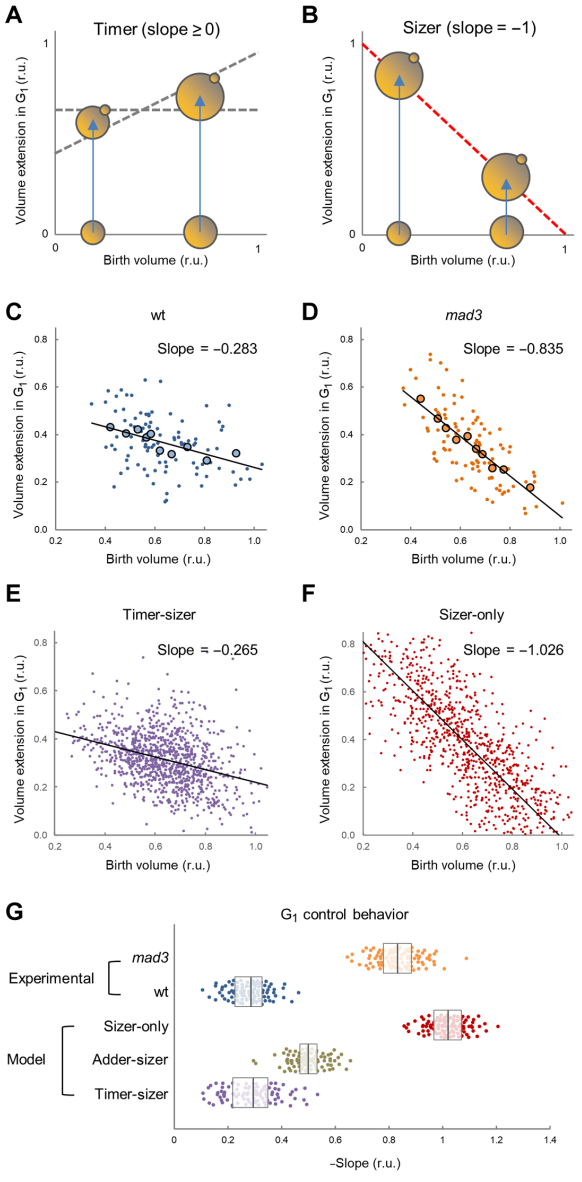


**Fig. 5. Mad3 tilts the sizer behavior of G1 control.** (**A** and **B**) Timer and sizer mechanisms in $G_1$ control. If $G_1$ length is only determined by time (A), the increase in size from birth to budding should be greatly independent of the birth size and produce a null or positive slope depending on whether linear or exponential growth in $G_1$ is considered. By contrast, if $G_1$ length only depends on the time required to reach a critical size (B), then cells born with a smaller size than average would have to increase their size to a larger extent than others, i.e., cell volume extension during $G_1$ should negatively correlate with birth volume (slope, −1). (**C** and **D**) Cell volume extension in $G_1$ as a function of birth volume in wild-type (wt, C) and Mad3-deficient (mad3, D) cells. Relative single-cell data ($N = 100$, small circles) are plotted. Mean values of binned data ($N = 10$, large circles) and the corresponding regression lines are also shown. (**E** and **F**) Simulations of the cell volume extension in $G_1$ as a function of birth volume in the mixed timer-sizer (E) or sizer-only (F) models. Relative single-cell data ($N = 1000$, small circles) are plotted. Mean values of binned data (large circles) and the corresponding regression lines are also shown. (**G**) $G_1$ control behavior of wild-type (wt) and Mad3-deficient (mad3) cells as measured by the absolute value of the slope from volume extension versus birth volume data. Bootstrapped values ($N = 100$) with the corresponding median and quartile values are plotted. Simulations produced from sizer, timer-sizer, and adder-sizer models are also shown.

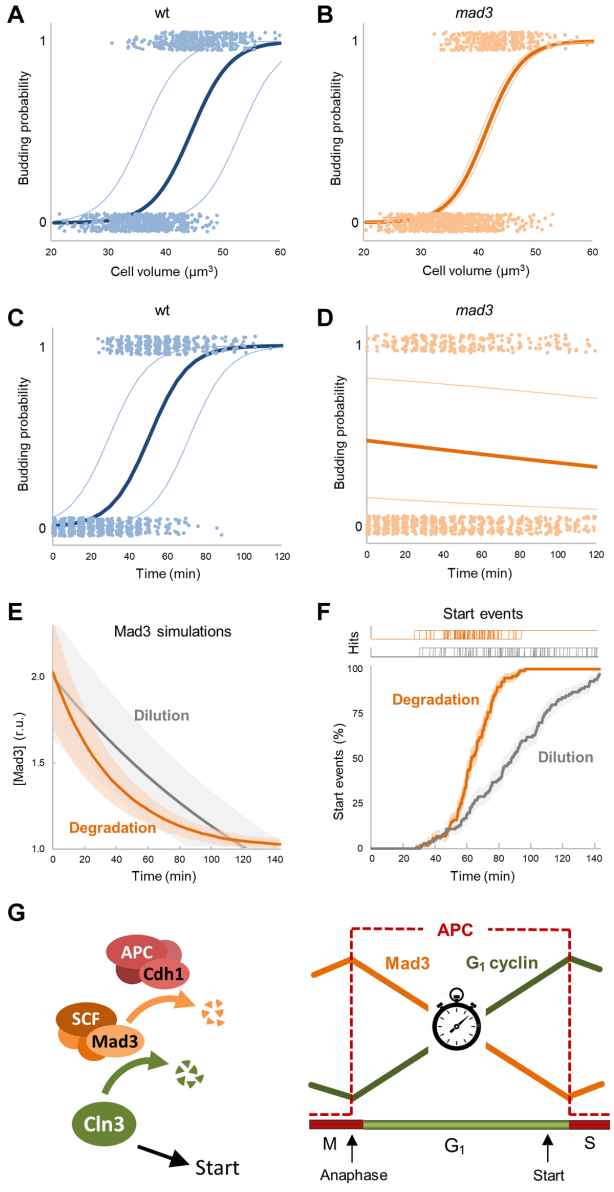


**Fig. 6. Mad3 as a timer mechanism in $G_1$ cyclin activation at Start.** (**A** to **D**) Logistic regression analysis of cell volume (A and B) and time from birth (C and D) as predictors of cell budding in wild-type (A and B) and Mad3-deficient (C and D) cells. Data from sampled time frames ($N = 1000$, small dots) of cells growing in $G_1$ are plotted with the corresponding logistic regression curves (mean ± SD). (**E**) Simulation of the decrease in Mad3 levels by degradation or dilution as deduced from experimental data on protein half-life and mass doubling time, respectively. The experimental coefficient of variation of mCh-Mad3 in cells at birth was used to obtain single trajectories ($N = 100$) and the resulting mean ± SD values are plotted. (**F**) Simulation of the time needed to reach a Mad3 threshold equivalent to 60% of the mean value at cell birth. Experimental parameters were as in (A), and the resulting mean frequencies ± SE values are plotted. Individual events (hits) are also shown at the top. (**G**) Intertwined degradation machineries are coupled to modulate $G_1$-cyclin activity for timely execution of cell cycle entry. Degradation of cyclin Cln3 depends on Mad3, which, in turn, is degraded by APC. Hence, because of the activation of APC in anaphase, Mad3 levels decrease with time during the subsequent $G_1$ phase, thus allowing the progressive accumulation of Cln3 in the nucleus to trigger Start. Once it entered the cell cycle, high Cdk activity turns off APC and Mad3 levels are allowed to recover until anaphase, which boosts again $G_1$-cyclin degradation to high levels before a new cycle is initiated.

equally effective. To this end, we simulated the decrease in Mad3 levels by degradation or dilution as deduced from experimental data on protein half-life (*43*, *48*) and mass doubling times, respectively. Applying the experimental coefficient of variation of mCh-Mad3 in cells at birth, we observed that Mad3 levels rapidly converged by degradation but not by dilution when $G_1$ progression was simulated (Fig. 6E). As a consequence, only degradation upshift predicted reaching a threshold in a range of times compatible with experimental $G_1$ lengths (Fig. 6F).

## DISCUSSION

$G_1$ cyclins are highly unstable (*49*, *50*), and this property allows cells to rapidly down-regulate their levels after transcriptional shut-off and, hence, quickly prevent entry into the cell cycle as a response to unfavorable conditions. In budding yeast, whereas $G_1$ cyclins are unstable throughout the cell cycle (*51*), the overall levels of Cln3 display a slight but significant increase during $G_1$ under nonperturbed conditions (*52*). Despite the relevance of degradation in cyclin regulation, its modulation during $G_1$ progression and cell cycle entry has not been analyzed. By using a partially stabilized hypoactive cyclin that allows live single-cell analysis (*22*, *33*), we found that the nuclear concentration of Cln3 increases as cells progress in $G_1$ and reaches a maximal level at cell cycle entry. As a consequence, Cln3 increased nuclear import and triggered accumulation of Cdc28 in the nucleus during mid-$G_1$ to reach a plateau later at Start that displayed a strong correlation with Whi5, the key inhibitor of the $G_1$-S regulon. We also found that Cln3 degradation by SCF is reduced as cells progress in $G_1$ in a Mad3-dependent manner. Mad3 levels, in turn, decreased during $G_1$ by APC-mediated degradation, thus defining a new layer for $G_1$ control (Fig. 6G).

While synthesis of Cln3 is assumed to be the key mechanism sensing the nutritional (*53*–*57*) and metabolic (*41*) status of the cell, modulation of Cln3 activity by growth rate, stress, and aging would be exerted at chaperone-dependent steps of protein folding and from the endoplasmic reticulum (ER) release (*26*–*29*). Regarding the specific physiological roles of the Mad3-based mechanism described here, we propose that Mad3 acts as a timer component in the Start network, thus explaining a long-standing question in cell size control. Wild-type cells of budding yeast display a negative correlation between cell volume extension and birth volume (*13*, *14*), but the observed slopes are at odds with the theoretical −1 value produced by the sizer mechanism. This important discrepancy has been attributed to different factors such as noise in the Start network (*12*, *13*) and single-cell variability in growth rate (*14*). Here, we show that, compared to wild-type, Mad3-deficient cells display a slope very close to that predicted by the pure sizer model, indicating that Mad3-dependent degradation of Cln3 counteracts the sizer properties of other mechanisms of $G_1$ control such as dilution of Whi5 (*11*, *22*). Nevertheless, the negative correlation of cell volume extension with birth volume in cells lacking Mad3 displayed a median slope (−0.827) significantly different from −1, which suggests that other factors and/or a noisy molecular design of the Start network also contribute to reduce the sizer behavior in $G_1$ control.

The dynamic properties of Mad3 down-regulation by APC are perfectly compatible with a timer mechanism. The half-life of Mad3 is ca. 30 min in $G_1$, which makes it possible to decrease its steady-state levels about twofold in 60 to 70 min, and cause relevant changes in Cln3 stability during the time period spent by cells in $G_1$ phase.

Mad3 may increase the binding affinity of Cdc4 for Cln3, or the intrinsic rate of ubiquitination once the $G_1$ cyclin is bound to SCF. The latter possibility would set Cln3 degradation in a cell size–independent manner, reinforcing Mad3 as a timer modulator of Start. In this regard, Mad3 could also modulate the role of Cdc4 on the stability of Cln1 and Cln2 in the nucleus (*38*), thus impinging on the positive feedback loop driven by these two $G_1$ cyclins to inactivate Whi5 (*58*).

We found that the total amount of Mad3 segregated 1:1 during cell division, but because of their smaller size, daughter cells initiate their cycle with a higher Mad3 concentration. This feature provides an additional daughter-specific mechanism to modulate Start (*59*). Although Mad3 has been shown to interact with kinetochore components of the spindle-assembly checkpoint, its presence is not restricted to centromeres and displays a diffuse pattern in the nucleus that is maintained throughout mitosis. Thus, the question remains as to how Mad3 attains equal segregation. As a possibility, very dynamic nonsaturating interactions with kinetochore (Bub1 and Scm3) or DNA binding (Ccr4 and Sin4) proteins could uncouple Mad3 scaling from cell size at division as shown for stably chromatin-bound proteins (*60*).

The reason why Start is not only controlled by a timer may reside on the fact that making $G_1$ length a constant parameter would preclude size homeostasis if exponential growth is assumed. In this case, cells born larger would grow faster and differences in cell size would increase with time. On the other hand, if only a sizer mechanism operated, cells displaying very low growth rates would spend much longer periods of time in $G_1$ and, hence, would be strongly counterselected in populations with intrinsic growth-rate variability. Thus, a timer component in $G_1$ control would particularly assist slow growing cells to execute Start despite being smaller than the critical size and would provide an explanation to our previous finding that cell size at Start is modulated by growth rate at the single-cell level (*14*).

In Whi5-deficient cells, the abovementioned slope drops to −0.2, indicating that the sizer mechanism is considerably compromised (*13*). However, cells lacking or expressing constant levels of Whi5 display similar cell size population variabilities compared to wild-type cells (*61*, *62*), suggesting that other mechanisms contribute to maintain cell size within limits. In this regard, differential scaling of transcription with cell size affecting inducers and inhibitors of cell cycle entry has been proposed as a complex sizer mechanism (*63*).

Mad3 mutant cells are only slightly smaller compared to wild-type cells. We have shown here that lack of Mad3 produces constant levels of nuclear Cln3 throughout $G_1$, similar to those attained at Start by wild-type cells. If this were the only mechanism upholding entry into the cell cycle, then Mad3-deficient cells should be very small. However, considering that Start is triggered when a threshold ratio between Cdc28 and Whi5 is attained in the nucleus, Whi5 would still delay Start unless sufficiently diluted by growth to the normal critical size (*22*). The recent finding that the Cdc28-Cln3 complex phosphorylates the RNAPolII C terminus to activate transcription of a subset of the $G_1$-S regulon genes (*19*), including *CLN1* and *CLN2*, suggests that Cln3 and Whi5 would work in successive but different substeps of Start. This order of function could explain the observed epistatic interaction between *MAD3* and *WHI5*. Moreover, the Mad3-Cln3 timer and Whi5 sizer mechanisms could act in a largely independent but synergistic manner, providing the Start network with a more robust design.

Although the underlying molecular basis remains unclear, the combined participation of sizer with timer or adder factors may also control proliferation in bacterial and mammalian cells. In bacteria, while DNA replication is initiated at a constant size, a growth rate–dependent time sets cell division (*64*). On the other hand, in an exhaustive analysis of mammalian cell lines, cell cycle time was proposed as an important modulator of cell size (*16*). Our results on the negative correlation of cell volume extension with birth volume in wild-type cells are better explained by the addition of a timer component compared to the mixed adder-sizer device. In addition, the mechanistic and kinetic properties of Mad3-based degradation of Cln3 strongly support the role of Mad3 in a timer mechanism. The contribution of the timer component could largely depend on the specific growing conditions, particularly on growth rate. Thus, cells slowly progressing through $G_1$ in the mouse epidermis offer a strong sizer behavior (*65*). By contrast, as a result of the timer component, rapidly growing cells would adapt their size to growth rate.

Last, we also show that an exceeding number of centromeres causes increased levels of Mad3 in newborn cells, which would explain the observed faster degradation of Cln3 in $G_1$ phase and the larger budding size compared to control cells (*39*). We attribute the increase in Mad3 levels to the delay in the metaphase/anaphase transition, and APC activation, caused by tensionless kinetochores in centromeric vectors (*66*). When cells encounter difficulties in mitosis and become larger at birth, increased levels of Mad3 would prevent their premature entry into the subsequent cycle and ensure pre-replicative complex assembly. Thus, Mad3 would constitute a mother-to-daughter memory factor for cell size determination, perhaps also transmitting information on ploidy. The role of a chromosome-bound Cdk inhibitor in plants (*67*) suggests that size-independent mechanisms operate throughout evolution in cell cycle entry. As it would be likely stabilized by down-regulation of Fbl17 in response to DNA damage (*68*), this Cdk inhibitor could also act as a memory factor transmitting information of DNA synthesis and/or mitotic defects to the next $G_1$ phase in plant cells. We envisage that Mad3 degradation kinetics would have been evolutionarily optimized to set the most appropriate $G_1$ length and, perhaps more importantly, to diversify cell dimensions in unpredictable environments.

## MATERIALS AND METHODS

### Strain constructions

Yeast strains used in this study are listed in table S1. Methods for chromosomal gene transplacement and polymerase chain reaction–based directed mutagenesis have been described (*14*, *32*, *53*). Unless stated otherwise, all gene fusions were expressed at endogenous levels at their respective loci. C-terminal fusions of fluorescent proteins to Cdc28 (*69*), Whi5 (*22*), or Htb2 (*58*) have been previously characterized. The N-terminal mCitrine $Cln3^{11A}$ fusion protein contains a hypoactive and hyperstable cyclin with 11–amino acid substitutions (R108A, T420A, S449A, T455A, S462A, S464A, S468A, T478A, S514A, T517A, and T520A) that allows its detection by fluorescence microscopy with no gross effects on cell cycle progression (*22*). Fusion of mCherry to the N terminus or C terminus of Mad3 under the endogenous promoter decreased protein expression levels, likely because of the uncoupling of uncommon downstream transcriptional elements. Moreover, the C-terminal fusion did not accumulate in the nucleus as shown for wt Mad3 by immunofluorescence (*31*), suggesting that Mad3 mislocalization would affect protein stability.

Thus, since we wanted to analyze posttranscriptional changes on Mad3 levels during the cell cycle, we opted for using an N-terminal fusion under the constitutive *GPD1* promoter at the *MAD3* locus. Similarly, the N-terminal GFP-Cdc4 fusions were expressed from the constitutive *TEF1* promoter at the corresponding locus. Gene fusions and specific constructs requiring multiple fragments were obtained by one-step recombination in yeast cells as described (*70*).

### Growth conditions

Cells were grown under exponential conditions for seven to eight generations in synthetic complete (SC) medium with 2% glucose at 30°C before microscopy unless stated otherwise. Other carbon sources used were 2% galactose and 2% raffinose. Where indicated, cycloheximide was added at 20 μg/ml. Small newly born cells were isolated from Ficoll gradients (*71*).

### Time-lapse microscopy

Cells were analyzed by time-lapse microscopy in 35-mm glass-bottom culture dishes (GWST-3522, WillCo) in SC-based media at 30°C essentially as described (*14*) using fully motorized Leica AF7000 or Thunder Imager microscopes. Time-lapse images were analyzed with the aid of BudJ (*14*), an ImageJ (W. Rasband, National Institutes of Health) plugin (www.ibmb.csic.es/en/department-of-cell-biology-dcb/spatial-control-of-cell-cycle-entry/#lab-corner) to obtain cell dimensions and fluorescence data. Volume growth rate in $G_1$ was obtained as described (*14*). Background autofluorescence from untagged cells was subtracted.

### Determination of cellular and nuclear concentrations of fluorescent fusion proteins

Wide-field microscopy is able to collect the total fluorescence emitted by yeast cells, and consequently, cellular concentration of fluorescent fusion proteins was obtained by dividing the integrated fluorescence signal within the projected area of the cell by its volume. Regarding the quantification of nuclear levels, since the signal in the nuclear projected area is influenced by both nuclear and cytoplasmic fluorescence, determination of the nuclear concentration required specific calculations (fig. S1A) as described (*28*). In confocal microscopy, the fluorescence signal is directly proportional to the concentration of the fluorescent fusion protein and required no further calculations. The nuclear compartment was estimated as described (*14*). Briefly, the center of the nucleus was set as the gravity center of pixels with a fluorescence 30% higher than the mean value, and the radius was obtained as 0.4 times the cell radius (*72*). This approach produced results that correlated well with those obtained by colocalization with Htb2-mCherry as a nuclear marker (*14*). Moreover, these procedures made unnecessary the coexpression of a tagged nuclear protein and helped minimize light-induced damage during growth. In some experiments (fig. S1, C and D), the nuclear compartment was delimited by means of histone Htb2-mCh.

### Nuclear import rate determinations by FLIP

To analyze nuclear import kinetics of Cdc28-GFP, a circle inscribed within the Htb2-mCherry nuclear region was repetitively photobleached at 488 nm while the cell was imaged every 0.5 s to record fluorescence loss under a Zeiss LSM 780 confocal microscope. After background subtraction, fluorescence data were corrected with those from a nonbleached cell, and fluorescence signals within nuclear and cytoplasmic areas were used to analyze import kinetics as described (*28*). Briefly, fluorescence signals within nuclear ($F_n$) and cytoplasmic ($F_c$) areas were used to obtain a nuclear to cytoplasmic ratio ($F_n/F_c$). At steady-state ratio, the import ($dF_n/dt$) and export ($dF_c/dt$) rates are in equilibrium (i.e., $dF_n/dt = dF_c/dt$), and $dF_n/dt = K_i.F_c - (K_e + K_b)F_n$ and $dF_c/dt = K_e.F_n - K_i.F_c$, where $K_i$, $K_e$, and $K_b$ are the import, export, and bleaching rate constants, respectively. Thus, $K_i.F_c - (K_e + K_b)F_n = K_e.F_n - K_i.F_c$, and $K_i = (F_n/F_c)(K_e + K_b/2)$. The bleaching rate constant was obtained from Htb2-mCherry fluorescence loss in the same cell, and the export rate constant from the recovery kinetics after nuclear FLIP as described (*28*).

### Mad3-Cdc4 interaction by FRET

Cells expressing mCh-Mad3 and GFP-Cdc4 were analyzed by FRET under a Zeiss LSM 780 confocal microscope. Briefly, GFP-Cdc4 was excited at 488 nm, and its emission was measured at 490 to 532 nm. Excitation of mCh-Mad3 was at 561 nm, and emission was measured at 563 to 695 nm. The FRET signal was measured at 563 to 695 when excited at 488 nm. The relative FRET efficiency was calculated as $(I_F - k_D \times I_D - k_A \times I_A)/I_A$, where $I_A$, $I_D$, and $I_F$ are the fluorescence intensities recorded from the acceptor, donor, and FRET channels and $k_A$ and $k_D$ are correcting acceptor cross-excitation and donor bleed-through constants, respectively. Background autofluorescence in all channels from untagged cells was subtracted. FRET efficiencies obtained from cells expressing Cdc4-GFP and Mad3-mCh, or GFP and mCh as control are shown in fig. S4C. First, the FRET efficiency between GFP and mCh was not significantly different from zero, and second, FRET produced by the Cdc4-GFP Mad3-mCh pair did not change much over a 10-fold range of acceptor fluorescence values.

### Cell size simulations in $G_1$

We modeled volume growth during $G_1$ progression in daughter cells following exponential kinetics with the following variables: initial volume ($V_i$), budding volume ($V_b$), $G_1$ length ($G_1$), and duplication time ($\tau$). When used as independent variables, they were parameterized with experimental average data and coefficients of variation shown in data file S1. We assumed that independent variables followed normal distributions, which were used to generate random stochastic values and to calculate the dependent variables depending on three different scenarios of $G_1$ control: sizer, timer, adder, timer-sizer, or timer-adder behaviors, as follows.

#### *Sizer*

Newborn cells were given $V_i$, $V_b$, and $\tau$ as independent variables, and the length of the $G_1$ period was calculated as $G_1 = \tau \times \ln_2(V_b/V_i)$.

#### *Timer*

Newborn cells were given $V_i$, $G_1$, and $\tau$ as independent variables, and the budding volume was obtained as $V_b = V_i \times 2^{(G1/\tau)}$.

#### *Adder*

Newborn cells were given $V_i$ and $\Delta V$ as independent variables, and the budding volume was obtained as $V_b = \Delta V + V_i$.

#### *Timer-sizer*

Budding volumes were calculated following timer and sizer behaviors as above, and assuming an equal contribution to the final budding volume, the mean value was taken.

#### *Adder-sizer*

Budding volumes were calculated following adder and sizer behaviors as above, and assuming an equal contribution to the final budding volume, the mean value was taken.

### Mad3 degradation simulations

We first parametrized Mad3 synthesis and degradation reactions to obtain a half-life of 60 min (*43*). To simulate Cdh1 activation in $G_1$, we increased the degradation constant by twofold (*43*, *48*) and followed Mad3 with time as a function of initial levels stochastically generated from normal distributions with a coefficient of variation experimentally determined from wild-type cells (Fig. 6E). For comparison, dilution of Mad3 was also modeled using experimentally determined mass-doubling times from wild-type cells. As an approximation to $G_1$ length, we used the time at which Mad3 levels decreased to 60% relative to cell birth by degradation or dilution (Fig. 6F).

### Statistical analysis

Sample size is always indicated in the figure legends. For single-cell data, median and quartile values are shown. Pairwise comparisons were performed with a Mann-Whitney *U* test, and the resulting *P* values are shown in the corresponding figure panels. Time-lapse data from single cells are represented as the mean value of the population along time, while the shaded area represents the SEM. Multivariable logistic regression using cell size and time from birth as predictors of budding was done using randomly sampled individual time frames from time-lapse experiments with small newborn cells growing in $G_1$. For each cell and time frame, cell volume and time from birth were determined and tested as predictors of budding in the next 30 min by fitting a logistic model. To obtain logistic regression curves of either cell volume or time from birth as single predictors, the other variable was fixed as the mean ± SD from all sampled time frames.

## SUPPLEMENTARY MATERIALS

Supplementary material for this article is available at https://science.org/doi/10.1126/sciadv.abm4086

View/request a protocol for this paper from *Bio-protocol*.

## REFERENCES AND NOTES


1. E. Wood, P. Nurse, Sizing up to divide: Mitotic cell-size control in fission yeast. *Annu. Rev. Cell Dev. Biol.* **31**, 11–29 (2015).
2. Y. Chen, B. Futcher, Scaling gene expression for cell size control and senescence in *Saccharomyces cerevisiae*. *Curr. Genet.* **67**, 41–47 (2021).
3. E. Zatulovskiy, J. M. Skotheim, On the molecular mechanisms regulating animal cell size homeostasis. *Trends Genet.* **36**, 360–372 (2020).
4. M. D'Ario, R. Sablowski, Cell size control in plants. *Annu. Rev. Genet.* **53**, 45–65 (2019).
5. C. Garmendia-Torres, O. Tassy, A. Matifas, N. Molina, G. Charvin, Multiple inputs ensure yeast cell size homeostasis during cell cycle progression. *eLife* **7**, e34025 (2018).
6. T. W. Spiesser, C. Kühn, M. Krantz, E. Klipp, Bud-localization of CLB2 mRNA can constitute a growth rate dependent daughter sizer. *PLoS Comput. Biol.* **11**, e1004223 (2015).
7. J. Zapata, N. Dephoure, T. Macdonough, Y. Yu, E. J. Parnell, M. Mooring, S. P. Gygi, D. J. Stillman, D. R. Kellogg, PP2ARts1 is a master regulator of pathways that control cell size. *J. Cell Biol.* **204**, 359–376 (2014).
8. L. H. Hartwell, M. W. Unger, Unequal division in *Saccharomyces cerevisiae* and its implications for the control of cell division. *J. Cell Biol.* **75**, 422–435 (1977).
9. G. C. Johnston, J. R. Pringle, L. H. Hartwell, Coordination of growth with cell division in the yeast. *Exp. Cell Res.* **105**, 79–98 (1977).
10. G. Facchetti, F. Chang, M. Howard, Controlling cell size through sizer mechanisms. *Curr. Opin. Syst. Biol.* **5**, 86–92 (2017).
11. F. S. Heldt, R. Lunstone, J. J. Tyson, B. Novak, Dilution and titration of cell-cycle regulators may control cell size in budding yeast. *PLoS Comput. Biol.* **14**, e1006548 (2018).
12. D. Chandler-Brown, K. M. Schmoller, Y. Winetraub, J. M. Skotheim, The adder phenomenon emerges from independent control of pre- and post-Start phases of the budding yeast cell cycle. *Curr. Biol.* **27**, 2774–2783.e3 (2017).
13. S. Di Talia, J. M. Skotheim, J. M. Bean, E. D. Siggia, F. R. Cross, The effects of molecular noise and size control on variability in the budding yeast cell cycle. *Nature* **448**, 947–951 (2007).
14. F. Ferrezuelo, N. Colomina, A. Palmisano, E. Garí, C. Gallego, A. Csikász-Nagy, M. Aldea, The critical size is set at a single-cell level by growth rate to attain homeostasis and adaptation. *Nat. Commun.* **3**, 1012 (2012).
15. G. Facchetti, B. Knapp, F. Chang, M. Howard, Reassessment of the basis of cell size control based on analysis of cell-to-cell variability. *Biophys. J.* **117**, 1728–1738 (2019).
16. C. Cadart, S. Monnier, J. Grilli, P. J. Sáez, N. Srivastava, R. Attia, E. Terriac, B. Baum, M. Cosentino-Lagomarsino, M. Piel, Size control in mammalian cells involves modulation of both growth rate and cell cycle duration. *Nat. Commun.* **9**, 3275 (2018).
17. M. Tyers, G. Tokiwa, B. Futcher, Comparison of the *Saccharomyces cerevisiae* $G_1$ cyclins: Cln3 may be an upstream activator of Cln1, Cln2 and other cyclins. *EMBO J.* **12**, 1955–1968 (1993).
18. C. Bertoli, J. M. Skotheim, R. A. M. de Bruin, Control of cell cycle transcription during $G_1$ and S phases. *Nat. Rev. Mol. Cell Biol.* **14**, 518–528 (2013).
19. M. Kõivomägi, M. P. Swaffer, J. J. Turner, G. Marinov, J. M. Skotheim, $G_1$ cyclin-Cdk promotes cell cycle entry through localized phosphorylation of RNA polymerase II. *Science* **374**, 347–351 (2021).
20. A. Johnson, J. M. Skotheim, Start and the restriction point. *Curr. Opin. Cell Biol.* **25**, 717–723 (2013).
21. P. Jorgensen, M. Tyers, How cells coordinate growth and division. *Curr. Biol.* **14**, R1014–R1027 (2004).
22. K. M. Schmoller, J. J. Turner, M. Kõivomägi, J. M. Skotheim, Dilution of the cell cycle inhibitor Whi5 controls budding yeast cell size. *Nature* **526**, 268–272 (2015).
23. K. M. Schmoller, J. M. Skotheim, The biosynthetic basis of cell size control. *Trends Cell Biol.* **25**, 793–802 (2015).
24. E. Garí, T. Volpe, H. Y. Wang, C. Gallego, B. Futcher, M. Aldea, Whi3 binds the mRNA of the $G_1$ cyclin CLN3 to modulate cell fate in budding yeast. *Genes Dev.* **15**, 2803–2808 (2001).
25. J. A. Yaglom, A. L. Goldberg, D. Finley, M. Y. Sherman, The molecular chaperone Ydj1 is required for the p34CDC28-dependent phosphorylation of the cyclin Cln3 that signals its degradation. *Mol. Cell. Biol.* **16**, 3679–3684 (1996).
26. E. Vergés, N. Colomina, E. Garí, C. Gallego, M. Aldea, Cyclin Cln3 is retained at the ER and released by the J chaperone Ydj1 in late $G_1$ to trigger cell cycle entry. *Mol. Cell* **26**, 649–662 (2007).
27. E. Parisi, G. Yahya, A. Flores, M. Aldea, Cdc48/p97 segregase is modulated by cyclin-dependent kinase to determine cyclin fate during $G_1$ progression. *EMBO J.* **37**, e98724 (2018).
28. D. F. Moreno, E. Parisi, G. Yahya, F. Vaggi, A. Csikász-Nagy, M. Aldea, Competition in the chaperone-client network subordinates cell-cycle entry to growth and stress. *Life Sci. Alliance* **2**, e201800277 (2019).
29. D. F. Moreno, K. Jenkins, S. Morlot, G. Charvin, A. Csikász-Nagy, M. Aldea, Proteostasis collapse, a hallmark of aging, hinders the chaperone-Start network and arrests cells in $G_1$. *eLife* **8**, e48240 (2019).
30. H. Wang, L. B. Carey, Y. Cai, H. Wijnen, B. Futcher, Recruitment of Cln3 cyclin to promoters controls cell cycle entry via histone deacetylase and other targets. *PLoS Biol.* **7**, e1000189 (2009).
31. K. G. Hardwick, R. C. Johnston, D. L. Smith, A. W. Murray, MAD3 encodes a novel component of the spindle checkpoint which interacts with Bub3p , Cdc20p , and Mad2p. *J. Cell Biol.* **148**, 871–882 (2000).
32. H. Wang, E. Garí, E. Vergés, C. Gallego, M. Aldea, Recruitment of Cdc28 by Whi3 restricts nuclear accumulation of the $G_1$ cyclin-Cdk complex to late $G_1$. *EMBO J.* **23**, 180–190 (2004).
33. X. Liu, X. Wang, X. Yang, S. Liu, L. Jiang, Y. Qu, L. Hu, Q. Ouyang, C. Tang, Reliable cell cycle commitment in budding yeast is ensured by signal integration. *eLife* **4**, e03977 (2015).
34. N. P. Edgington, B. Futcher, Relationship between the function and the location of $G_1$ cyclins in *S. cerevisiae*. *J. Cell Sci.* **114**, 4599–4611 (2001).
35. M. E. Miller, F. R. Cross, Mechanisms controlling subcellular localization of the G1 cyclins Cln2p and Cln3p in budding yeast. *Mol. Cell. Biol.* **21**, 6292–6311 (2001).
36. F. R. Cross, V. Archambault, M. Miller, M. Klovstad, Testing a mathematical model of the yeast cell cycle. *Mol. Biol. Cell* **13**, 52–70 (2002).
37. I. Quilis, J. C. Igual, Molecular basis of the functional distinction between Cln1 and Cln2 cyclins. *Cell Cycle* **11**, 3117–3131 (2012).
38. B. D. Landry, J. P. Doyle, D. P. Toczyski, J. A. Benanti, F-box protein specificity for G1 cyclins is dictated by subcellular localization. *PLOS Genet.* **8**, e1002851 (2012).
39. J. M. Martínez-Láinez, D. F. Moreno, E. Parisi, J. Clotet, M. Aldea, Centromeric signaling proteins boost $G_1$ cyclin degradation and modulate cell size in budding yeast. *PLoS Biol.* **16**, e2005388 (2018).
40. Z. Xie, K. A. Jay, D. L. Smith, Y. Zhang, Z. Liu, J. Zheng, R. Tian, H. Li, E. H. Blackburn, Early telomerase inactivation accelerates aging independently of telomere length. *Cell* **160**, 928–939 (2015).
41. A. Litsios, D. H. E. W. Huberts, H. M. Terpstra, P. Guerra, A. Schmidt, K. Buczak, A. Papagiannakis, M. Rovetta, J. Hekelaar, G. Hubmann, M. Exterkate, A. Milias-Argeitis, M. Heinemann, Differential scaling between $G_1$ protein production and cell size dynamics

promotes commitment to the cell division cycle in budding yeast. *Nat. Cell Biol.* **21**, 1382–1392 (2019).
42. P. T. Spellman, G. Sherlock, M. Q. Zhang, V. R. Iyer, K. Anders, M. B. Eisen, P. O. Brown, D. Botstein, B. Futcher, Comprehensive identification of cell cycle-regulated genes of the yeast *Saccharomyces cerevisiae* by microarray hybridization. *Mol. Biol. Cell* **9**, 3273–3297 (1998).
43. E. M. J. King, S. J. A. van der Sar, K. G. Hardwick, Mad3 KEN boxes mediate both Cdc20 and Mad3 turnover, and are critical for the spindle checkpoint. *PLOS ONE* **2**, e342 (2007).
44. A. Varshavsky, The N-end rule pathway and regulation by proteolysis. *Protein Sci.* **20**, 1298–1345 (2011).
45. E. McShane, C. Sin, H. Zauber, J. N. Wells, N. Donnelly, X. Wang, J. Hou, W. Chen, Z. Storchova, J. A. Marsh, A. Valleriani, M. Selbach, Kinetic analysis of protein stability reveals age-dependent degradation. *Cell* **167**, 803–815.e21 (2016).
46. P. Freire, P. Vinod, B. Novak, Interplay of transcriptional and proteolytic regulation in driving robust cell cycle progression. *Mol. BioSyst.* **8**, 863–870 (2012).
47. P. A. Fantes, Control of cell size and cycle time in *Schizosaccharomyces pombe*. *J. Cell Sci.* **24**, 51–67 (1977).
48. C. Liu, D. Van Dyk, V. Choe, J. Yan, S. Majumder, M. Costanzo, X. Bao, C. Boone, K. Huo, M. Winey, H. Fisk, B. Andrews, H. Rao, Ubiquitin ligase Ufd2 is required for efficient degradation of Mps1 kinase. *J. Biol. Chem.* **286**, 43660–43667 (2011).
49. J. Diehl, F. Zindy, C. Sherr, Inhibition of cyclin D1 phosphorylation on threonine-286 prevents its rapid degradation via the ubiquitin-proteasome pathway. *Genes Dev.* **11**, 957–972 (1997).
50. J. Yaglom, M. H. K. Linskens, S. Sadis, D. M. Rubin, B. Futcher, D. Finley, p34Cdc28-mediated control of Cln3 cyclin degradation. *Mol. Cell. Biol.* **15**, 731–741 (1995).
51. B. Schneider, E. Patton, S. Lanker, M. Mendenhall, C. Wittenberg, B. Futcher, M. Tyers, Yeast $G_1$ cyclins are unstable in $G_1$ phase. *Nature* **395**, 86–89 (1998).
52. R. A. Sommer, J. T. DeWitt, R. Tan, D. R. Kellogg, Growth-dependent signals drive an increase in early $G_1$ cyclin concentration to link cell cycle entry with cell growth. *eLife* **10**, e64364 (2021).
53. C. Gallego, E. Garí, N. Colomina, E. Herrero, M. Aldea, The Cln3 cyclin is down-regulated by translational repression and degradation during the $G_1$ arrest caused by nitrogen deprivation in budding yeast. *EMBO J.* **16**, 7196–7206 (1997).
54. L. L. Newcomb, D. D. Hall, W. Heideman, AZF1 is a glucose-dependent positive regulator of CLN3 transcription in *Saccharomyces cerevisiae*. *Mol. Cell. Biol.* **22**, 1607–1614 (2002).
55. M. Polymenis, E. V. Schmidt, Coupling of cell division to cell growth by translational control of the $G_1$ cyclin CLN3 in yeast. *Genes Dev.* **11**, 2522–2531 (1997).
56. N. Talarek, E. Gueydon, E. Schwob, Homeostatic control of START through negative feedback between Cln3-Cdk1 and Rim15/Greatwall kinase in budding yeast. *eLife* **6**, e26233 (2017).
57. S. Menoyo, N. Ricco, S. Bru, S. Hernández-Ortega, X. Escoté, M. Aldea, J. Clotet, Phosphate-activated cyclin-dependent kinase stabilizes $G_1$ cyclin to trigger cell cycle entry. *Mol. Cell. Biol.* **33**, 1273–1284 (2013).
58. J. M. Skotheim, S. Di Talia, E. D. Siggia, F. R. Cross, Positive feedback of $G_1$ cyclins ensures coherent cell cycle entry. *Nature* **454**, 291–296 (2008).
59. S. Di Talia, H. Wang, J. M. Skotheim, A. P. Rosebrock, B. Futcher, F. R. Cross, Daughter-specific transcription factors regulate cell size control in budding yeast. *PLoS Biol.* **7**, e1000221 (2009).
60. M. P. Swaffer, J. Kim, D. Chandler-Brown, M. Langhinrichs, G. K. Marinov, W. J. Greenleaf, A. Kundaje, K. M. Schmoller, J. M. Skotheim, Transcriptional and chromatin-based partitioning mechanisms uncouple protein scaling from cell size. *Mol. Cell* **81**, 4861–4875.e7 (2021).
61. P. Jorgensen, I. Rupes, J. R. Sharom, L. Schneper, J. R. Broach, M. Tyers, A dynamic transcriptional network communicates growth potential to ribosome synthesis and critical cell size. *Genes Dev.* **18**, 2491–2505 (2004).
62. F. Barber, A. Amir, A. W. Murray, A. W. Murray, Cell-size regulation in budding yeast does not depend on linear accumulation of Whi5. *Proc. Natl. Acad. Sci. U.S.A.* **117**, 14243–14250 (2020).
63. Y. Chen, G. Zhao, J. Zahumensky, S. Honey, B. Futcher, Differential scaling of gene expression with cell size may explain size control in budding yeast. *Mol. Cell* **78**, 359–370.e6 (2020).
64. M. Wallden, D. Fange, E. G. Lundius, Ö. Baltekin, J. Elf, The synchronization of replication and division cycles in individual *E. coli* cells. *Cell* **166**, 729–739 (2016).
65. S. Xie, J. M. Skotheim, A $G_1$ sizer coordinates growth and division in the mouse epidermis. *Curr. Biol.* **30**, 916–924.e2 (2020).
66. B. Futcher, J. Carbon, Toxic effects of excess cloned centromeres. *Mol. Cell. Biol.* **6**, 2213–2222 (1986).
67. M. D'Ario, R. Tavares, K. Schiessl, B. Desvoyes, C. Gutierrez, M. Howard, R. Sablowski, Cell size controlled in plants using DNA content as an internal scale. *Science* **372**, 1176–1181 (2021).
68. T. Pan, Q. Qin, C. Nong, S. Gao, L. Wang, B. Cai, M. Zhang, C. Wu, H. Chen, T. Li, D. Xiong, G. Li, S. Wang, S. Yan, A novel WEE1 pathway for replication stress responses. *Nat. Plants* **7**, 209–218 (2021).
69. H. Maekawa, T. Usui, M. Knop, E. Schiebel, Yeast Cdk1 translocates to the plus end of cytoplasmic microtubules to regulate bud cortex interactions. *EMBO J.* **22**, 438–449 (2003).
70. D. G. Gibson, G. A. Benders, K. C. Axelrod, J. Zaveri, M. A. Algire, M. Moodie, M. G. Montague, J. C. Venter, H. O. Smith, C. A. Hutchison III, One-step assembly in yeast of 25 overlapping DNA fragments to form a complete synthetic *Mycoplasma genitalium* genome. *Proc. Natl. Acad. Sci. U.S.A.* **105**, 20404–20409 (2008).
71. J. M. Mitchison, in *Yeast*, *A Practical Approach*, I. Campbell, J. Duffus, Eds. (IRL Press, 1988), pp. 51–64.
72. P. Jorgensen, N. P. Edgington, B. L. Schneider, I. Rupes, M. Tyers, B. Futcher, The size of the nucleus increases as yeast cells grow. *Mol. Biol. Cell* **18**, 3523–3532 (2007).

**Acknowledgments:** We thank E. Rebollo for technical assistance and J. Skotheim and F. Ferrezuelo for providing strains. We also thank C. Rose for editing the manuscript and C. Gallego for helpful comments. **Funding:** This work was supported by Agencia Estatal de Investigación Spain PID2019-109638GB-I00 (to M.A.), Agencia Estatal de Investigación Spain PGC2018-096597-B-I00 (to J.C.), Agència de Gestió d'Ajuts Universitaris i de Recerca Catalonia 2019FI_B 00452 (to A.P.P.), and Agència de Gestió d'Ajuts Universitaris i de Recerca Catalonia 2014FI_B 00074 (to D.F.M.). **Author contributions:** Conceptualization: J.C. and M.A. Investigation: A.P.P., M.H.A., and D.F.M. Data analysis: A.P.P. and D.F.M. Supervision: J.C. and M.A. Writing (original draft): J.C. and M.A. Writing (review and editing): J.C. and M.A. **Competing interests:** The authors declare that they have no competing interests. **Data and materials availability:** All data needed to evaluate the conclusions in the paper are present in the paper and/or the Supplementary Materials. BudJ can be obtained from www.ibmb.csic.es/en/department-of-cell-biology-dcb/spatial-control-of-cell-cycle-entry/#lab-corner.

Submitted 25 September 2021
Accepted 23 March 2022
Published 6 May 2022
10.1126/sciadv.abm4086